Morphological models of networks of inter-granules micropores: identification and validation based on 2D and 3D imaging

Léo Moutin, Christelle Duguay, Laurent Fayette, A. King, Renaud Masson, Michel Bornert

Morphological models of networks of inter-granules micropores: identification and validation based on 2D and 3D imaging

Léo Moutin[0000−0001−5962−831], Christelle Duguay[0000−0002−3931−4993], Laurent Fayette[0000−0002−1045−3201], Andrew King[0000−0001−8542−1354], Renaud Masson[0000−0002−6496−8120], and Michel Bornert[0000−0002−6964−5793]

Abstract In view of predicting the overall thermal conductivity of ceramics with a granular microstructure exhibiting complex networks of pores preferably located at the interfaces between granules, a simple microstructural model has been developed to capture the dominant features of such a specific morphology. Generated 3D virtual networks of pores are obtained as the intersection of a Voronoi tessellation, representing the granules, and a boolean model of monodisperse overlapping spheres [1]. The two non-dimensional parameters fully determining such networks have been first adjusted so as to reproduce at best some morphological properties extracted from 2D optical images of various real samples [2]. To further validate this model, several small samples of the same materials have in addition been imaged in 3D by synchrotron X-ray micro-computed tomography, with a specific setup adapted to the very strong attenuation of these ceramics. The consistency of the results measured in 2D on cross-sections of tomography images with those measured on optical microscopy images has been first checked. Next, qualitative comparisons between observed 3D pore networks and simulated ones with parameters adjusted from 2D observations have been complemented by more quantitative ones.

Léo Moutin
CEA, DES, IRESNE, DEC, Cadarache F-13018 Saint-Paul-lez-Durance e-mail: leo.moutin@cea.fr

Christelle Duguay
e-mail: christelle.duguay@cea.fr

Laurent Fayette
e-mail: laurent.fayette@cea.fr

Renaud Masson
e-mail: renaud.masson@cea.fr

Andrew King
Synchrotron Soleil, Psiché Beamline, L'Orme des Merisiers, F-91190 Saint-Aubin e-mail: king@synchrotron-soleil.fr

Michel Bornert
Laboratoire Navier, Ecole des ponts, Univ. Gustave Eiffel, CNRS UMR 8205, 6-8 avenue Blaise Pascal, Champs-sur-Marne, 77455 Marne-la-Vallée Cedex e-mail: michel.bornert@enpc.fr

1 Introduction

This work aims at predicting the thermal conductivity of porous uranium dioxide ceramics manufactured by sintering multi-crystalline granules. These materials exhibit complex networks of elongated pores preferably located at the interfaces between granules, with features depending on the manufacturing process. Because such microcracks-like pores act as strong barriers to heat propagation, accounting for the specific geometry of such pore networks is essential for accurate predictions.

Among the various methodologies for modelling microstructures (see e.g. the review in [3]), the adopted model, detailed in [1], is based on probabilistic approaches to generate random sets in 3D, in line with [4]. More specifically, following [5], it combines two random sets to constrain the geometric location of cracks, as in [6] for another case of cracked polycrystals. Following [7] who adopted a similar approach for cold spray coatings, the parameters of this 3D model could be adjusted in [2] so as to reproduce at best some morphological properties measured from 2D images from optical microscopy (OM) of real samples, appropriately filtered to extract the major thermal barriers at granules interfaces, without excessive details nor smoothing.

The 3D model finally obtained was thus tuned on 2D information only. The here-presented contribution extends its validation through comparisons with 3D images of the same real materials obtained by X-ray computed microtomography (XRCT). The experimental procedure to obtain and process these data and to perform these comparisons are presented in section 4 after a brief review of the adopted morphological model (section 2) and its tuning to various materials based on 2D data (section 3).

2 A simple morphological model of inter-granules pore networks

The adopted virtual microstructures describing networks of cracks located at inter-granules boundaries (IGB) are generated by combining two random sets [1]. The first one corresponds to the IGB and is obtained from a Voronoi tessellation of seeds resulting from the random sequential adsorption (RSA) of monodisperse spheres, with periodicity conditions.The used algorithm allows to almost reach its theoretical saturation with reasonnably short simulation times, so that the obtained tessellation exhibits rather homogeneous grain sizes. The second random set is obtained by randomly distributing monodisperse spheres, so-called delimiting spheres, over the simulation domain using a standard Poisson point process for their centers, providing a boolean model of spheres. The virtual microstructure of inter-granules pores is finally obtained by keeping the IGB not contained in the delimiting spheres.

This simple method has three input parameters: the radius R_g of the spheres of the RSA model, the radius R_l of the delimiting spheres and the density d_l of the Poisson process. Because of scale invariance, the effective thermal conductivity only depends on two non-dimensional parameters: the ratio R_l/R_g and the volume fraction of the boolean model defining the delimiting spheres. It can be computed through full-

field simulations techniques, such as the FFT method (see implementation details in [1]). By varying these parameters, a wide variety of microstructures could be generated (illustrative examples are provided in figure 1) with significantly different effective thermal conductivities. The latter were also compared to those of uniformly weakened solids, with cracks randomly distributed over the bulk, at similar overall densities. It was observed that the concentration of pores on the IGB causes a significant reduction in effective thermal conductivity.

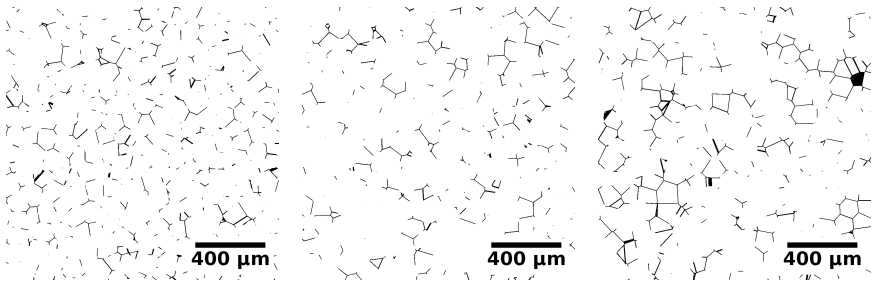

Fig. 1 Virtual microstructures obtained using the method introduced in [1] for various parameters choices. From left to right: $R_l/R_g = 0.7$, $R_l/R_g = 1.25$ and $R_l/R_g = 1.5$.

3 Tuning parameters to real materials

A number of model materials with various microstructures have been fabricated to investigate the relationship between porosity and thermal properties. The manufacturing conditions were varied to obtain samples over a wide range of porosity. Among these many samples, focus will be given in the following to three of them, denoted C_1, C_2 and C_3. They exhibit increasing open porosity volume fractions: $c_1^o = 0.9\%$, $c_2^o = 1.1\%$ and $c_2^o = 3.45\%$, which cover the full porosity range of interest for the practical application. Due to their slender shape, interconnections of inter-granules pores in the volume are expected so that the open porosity is in practice well correlated with the inter-granules porosity. The aim is now to adjust the parameters of the simple model proposed in [1] to such real materials and then check its capability to reproduce sufficiently accurately the real porous networks, both in terms of their morphological characteristics and their thermal properties. We summarize in this section the methodology proposed in [2] to tune the parameters of the model so that it simulates a pore network representative of a given real ceramic.

First, based on 2D OM high definition images of large areas of samples properly prepared to reveal porosity, we characterize the porous networks of the studied ceramics in order to extract some descriptor parameters. To this end, an image processing protocol has been developed to clearly isolate and simplify the description of the objects of interest that are, in our case, the inter-granules pores. This image

processing protocol consists of four main operations, to go from a raw OM image to a skeletonized (i.e. objects with one pixel thickness) binary image. They involve appropriate filtering to eliminate irrelevant details without over-smoothing (see [2] for details). The obtained topological skeleton encodes the main geometrical features of the inter-granule pore network and we focus on the following four quantities to characterize it. The density of the crack network of the ceramics is quantified using the length of the intercepts (l_{Inter}) [8]. To assess the size distribution of the inter-pore space, we use the principles of Matheron's granulometry [9]: we consider for each pixel in the solid phase the radius of the largest circle (r_{Mat}) that can be inserted between the skeleton and contains this pixel. The lengths of the cracks are characterized by estimating two quantities, namely the "lengths of the branches" (l_{bra}) and "the lengths of the primary branches" (l_{braPrim}) of the skeletons. The "branches" are defined as the linear objects obtained after eliminating the connection points where these objects meet in the skeleton and the "primary branches" the linear objects retained to quantify the geodesic diameter of the connected components of the skeleton. The cumulative statistical distributions of these quantities (H_{Inter}, H_{Mat}, H_{bra} and H_{braPrim}), weighted either by surface of number, are considered for a detailed description of the porous microstructures[1].

This quantitative characterization of the porous network of a given ceramic provides the input data of an automated optimization procedure that aims at producing a tuned virtual microstructure, of which the above descriptor parameters, measured on 2D cross-sections of the 3D generated microstructures, are required to be as close as possible to their measured counterparts. The missmatch function to be minimized by this procedure is the average of the discrepancies for each of the four cumulative distributions (discretized over control points) with more weight given to the length of the branches and the primary branches, for practical reasons [2]. As a qualitative illustration of the results, 3D renderings of the obtained tuned virtual microstructures are given in figure 5. For the tested ceramics, the developed optimization algorithm gives satisfactory quantitative results as the cumulative distributions of the four descriptor parameters of the tuned microstructures and of the real ceramics are in good agreement (figure 2). One can however notice that the fitting of Matheron's 2D granulometry is less good than for the other quantities, especially for the larger scales. A possible explanation is that the selected scheme for the IGB generates a narrow grain size distribution and flat and rather regular boundaries. A modified point process for its seeds, or the use of Laguerre polyhedra or even locally anisotropic tessellations could provide the required degrees of freedom for a better fit, but at the price of a more complex model, involving more parameters.

To further validate this 2D identification process, full-field 2D numerical simulations (based on the FFT method) were performed on both processed OM images of the studied ceramics and cross-sections extracted from the tuned 3D microstructures. These 2D simulations are used as an additional validation of the fitted model, including not only the partial set of 2D morphological features used to fit the model, but also the full set of features determining the thermal properties of a 2D heterogeneous

[1] Note that cumulative distributions are more convenient than distribution functions for subsequent optimization because they are more regular.

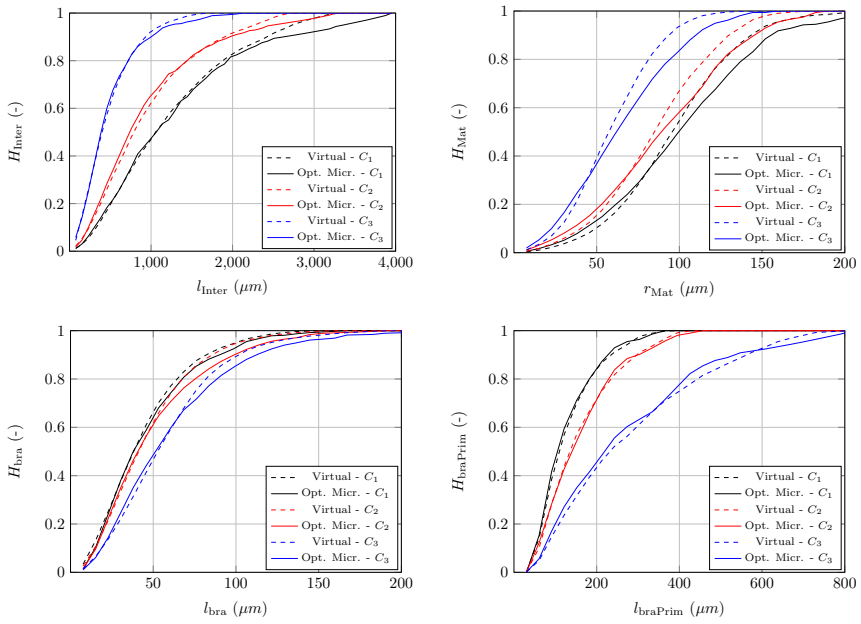

Fig. 2 Cumulative distributions associated with each descriptor parameter obtained on the reference ceramics and on the tuned microstructures (from [2]).

medium. Of course, this is not sufficient to validate the performance of the model in terms of full 3D thermal properties, but it does provide an additional and original means to confirm the similarity between the virtual and real 2D cross-sections. This validation was carried out on the effective 2D properties, but also and above all on the local field statistics in terms of distribution functions and spatial correlations. These simulations have allowed us to highlight a good correspondence in the 2D thermal behaviour of the virtual and real microstructures [2].

4 Validation on 3D geometric experimental data

The methodology for generating representative virtual microstructures described in [2] and recalled in the previous section is based on 2D images of the porous network of the ceramics of interest. Obviously, the relevance of the model in reproducing the 2D characteristics of the porous network and its efficiency in predicting 2D thermal properties is not sufficient to fully validate the relevance of the model for simulating the real (3D) properties of the ceramics under consideration. For this reason, and in order to obtain 3D images of the porous network of the real ceramics, an X-ray tomography campaign was carried out on the Psiché beamline at Synchrotron Soleil (Saint Aubin, France), on some representative model samples.

4.1 Synchrotron X-ray tomography imaging of porous UO_2 ceramics

Absorption X-ray computed tomography (XRCT) is a non destructive 3D imaging technique based on the attenuation of X-rays by matter. Radiographs of the sample along many directions, recorded by a 2D detector, serve as input data of a mathematical inversion algorithm which outputs a 3D image in which grey levels code the local attenuation coefficient of the constitutive material. This technique is well suited to image non absorbing pores in a matrix, as they induce a strong contrast, under the conditions that the spatial resolution of the radiographs is sufficiently high with respect to pore size. In addition, the energy of the probing X-rays needs to be adapted to the size of the sample and the attenuation properties of its constituents, which strongly increase with density and atomic number. The highly absorbing UO_2 ceramics under consideration (density of 10.96 g/cm^3) with inter-granules pores of micrometric thickness require thus rather non-conventional conditions for their XRCT imaging. They could be provided by the Psiché beamline, in particular thanks to its wiggler which generates a wide spectrum of radiations, with intense flux still available above 100keV. Another difficulty to be faced was the radioactivity of the samples, which required to limit their size and to keep them in sealed aluminum sample holders all along the experiment, in order to comply with safety regulations.

To comply with all these constraints, small cylindrical samples were cored with a diameter of 1.2 mm and a height of 1.3 mm. Photons with energy below 65keV were removed with appropriate filters but the full high energy spectrum of the wiggler beam was kept. Under such conditions, the photon flux transmitted through the full diameter of the sample was maximal at about 90keV, but represented only about 5% of the incoming flux. With standard scanning procedures, this would have induced very strong contrast in the radiographs, and very poor signal to noise ratios to avoid saturation on their edges. That's why the beam profiling technique proposed in [10] was adopted: a specific copper filter, in which five cylindrical holes having the size of the sample and aligned with it were drilled, was placed in the beam before the sample so that the total attenuation was almost uniform over the radiographs, which could therefore be recorded with sufficiently low noise levels and in reasonable times. Reference images, recorded with the filter but without the sample, had however to be averaged more intensively than for standard conditions, but without significantly increasing the total scanning time. The LuAg scintillator with a thickness of 100μm was imaged with a microscope with a $\times$10 optical magnification by an ORCA digital camera with a 6.5μm pixel size. The reconstructed 3D images, performed with the PyHST software, had thus a voxel size of 0.65μm. This is significantly smaller than the pixel size of 1.52μm of the OM images used for the 2D characterization of the pore network (see previous section), but the actual spatial resolution of the 3D images is indeed somewhat poorer than this nominal voxel size. Total scan time for a sample was about 90 minutes and 24 samples could be imaged during a 4 days campaign, among which samples of the three materials under consideration here. Several filtering operations, not detailed here, had to be applied to the obtained 2048^3 voxels images to remove ring artefacts and non-standard beam-hardening effects induced by the beam profiling technique.

4.2 Comparison between OM images and XRCT cross-sections

Before characterising the porous network using the full 3D XRCT data, a preliminary study was carried out to check the consistency of the results measured in 2D on cross-sections of XRCT images with those measured on OM images. The 2D image processing protocol introduced in section 3 to characterize OM images was therefore also applied to such XRCT cross-sections of same orientation. In order to threshold the XRCT images at a greylevel similar to the one used to binarize the OM images, the intrinsic grey levels of the matrix and pores phases was determined in both the XRCT and OM images. The threshold for XRCT images was then set at the same relative level between matrix and pores grey levels as the one used to segment the OM images. Figure 3 shows a cross-section of an XRCT and an OM image with the same observation window size. These images were taken on the C_3 ceramic and show the segmented pores, the inter-granules pore skeletons and their primary branches. The visual comparison between these images emphasises the good qualitative consistency between the pore networks identified with both imaging techniques.

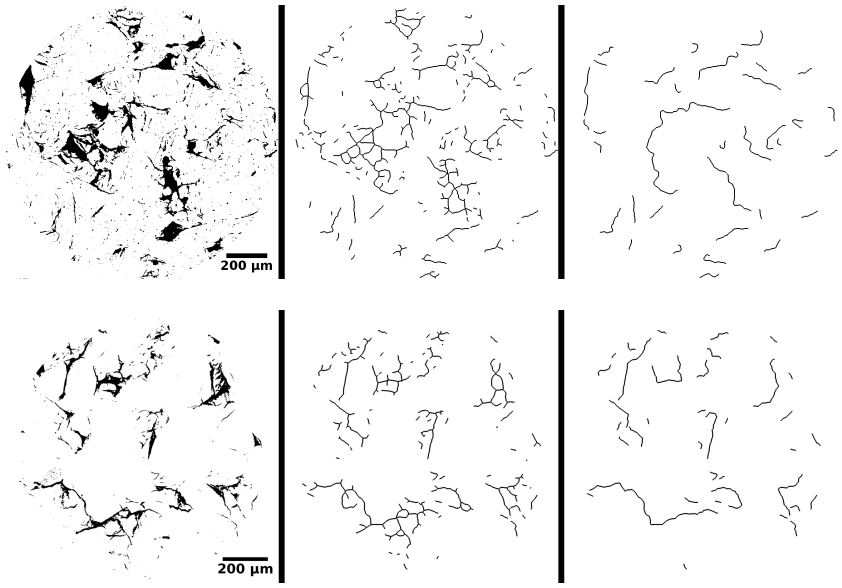

Fig. 3 Comparison of an OM image (top) and a radial section of a XRCT image (bottom) of ceramic C_3 using the observation windows of same size and identical image processing protocols: segmented pores (left), inter-granules pore skeletons (centre) and their primary branches (right).

For a more quantitive comparison, two of the descriptor parameters introduced in section 3 are considered again, namely the cumulative distribution functions associated with branches lengths and primary branches lengths. As XRCT windows are small, for the reasons explained in previous sections, some bias might be expected

because of edge effects. This occurs when the size of the window is not large enough compared to the size of the objects being characterized, particularly when no special treatment is applied to objects that are cut at the edges. Such treatments are not necessary for the 2D analyses on the full OM images as they are sufficiently large. For simplicity we did not implement them either for the smaller windows, but performed the same (biased) analysis on XRCT cross-sections and sub-windows of same size extracted randomly from the complete large OM images, as in figure 3, which ensures a valid quantitative comparison. For a better statistically representativity, the parameters are in addition measured over several windows: different sampling areas for the OM images and different slices for the XRCT ones.

Results are plotted in figure 4. For C_1 and C_3, the cumulative distribution functions H_{bra} and H_{braPrim} measured on the OM and XRCT images are close. This underlines the good quantitative coherence of the porous network observed by OM and XRCT. However, the comparison is less satisfactory for H_{braPrim} in the case of the C_2 ceramic. A possible explanation is that the small XRCT volumes may not adequately capture possible long range spatial variations in the morphology of the pore network. To quantify such spatial variations, we also measured the average differences between H_{bra} and H_{braPrim} obtained separately from all observation windows of the OM images. They are represented as uncertainty bars in figure 4. It is clear, especially for the primary branches of C_1 and C_2, that these variations are rather large, which lends weight to the above hypothesis: the XRCT result for H_{braPrim} for C_2 lies within the range of possible values measured by OM over similar sized windows. Note that the present discussion has been focused on the length of branches and primary branches, as these parameters are difficult to translate into 3D, but that similar results were obtained for the length of intercepts and Matheron's granulometry. These comparisons globaly confirm that 2D data extracted from OM surface measurements are consistent with 2D data extracted from the bulk of the material. There is in particular no significant bias due to surface preparation. On the other hand, they also show the limitations of XRCT images which are, at least for the considered ceramics, restricted to small window sizes and may not capture longer range effects.

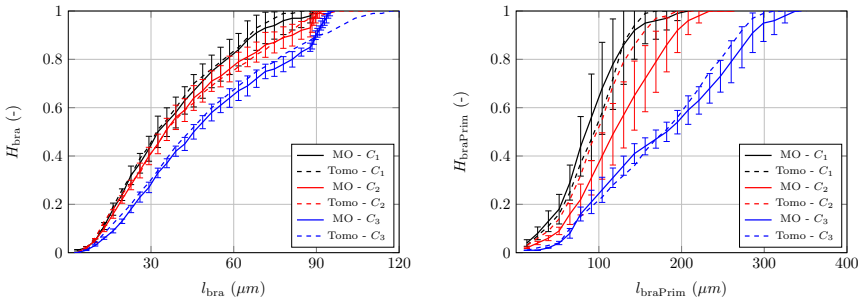

Fig. 4 Cumulative distribution functions associated with the length of branches (left) and the length of primary branches (right) measured on sub-windows of OM images reduced to the size of XRCT images and on sections of XRCT images. Bars quantify the spatial fluctuations of these functions when the observation window is randomly chosen in the large OM images.

4.3 3D image processing and characterization

We now turn to the characterization of the pore network in the ceramics of interest using the 3D data of XRCT images. Thresholding in 3D is performed as in previous section, but the removal of the smaller connected objects not belonging to the inter-granules pore network is now performed based on their 3D properties. A criterion relative to their sphericity[2] is selected, based on the fact that the inter-granules pores are long and slender as opposed to the smaller isolated objects, which are more spherical. Note that a circularity criterion served to filter pores in OM images. By studying the evolution of the sphericity of the objects as a function of their volume, it appears that eliminating objects with a sphericity above 0.2 is a good criterion for isolating the inter-granules pores. The extent of the obtained pore network, depicted as 3D surface renderings in the bottom of figure 5, visually appears to be consistent with their open porosity ($\approx 1\%$ for C_1 and C_2, and $\approx 3.5\%$ for C_3).

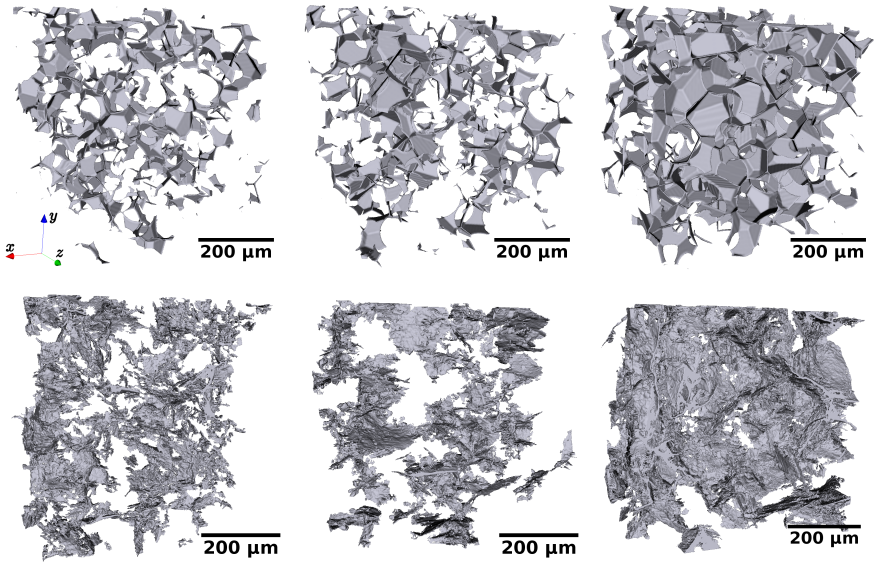

Fig. 5 3D illustrative views of local volumes ($\approx$ 650x650x650 µm^3) in the tuned virtual microstructures (top) and in the porous network extracted from XRCT images (bottom) associated respectively with the three ceramics C_1, C_2 and C_3 (from left to right).

In order to characterize the porous network in 3D, two of the descriptor parameters introduced in section 3 are used again, namely the length of the intercepts (defined as in 2D but extended over 3D images) and Matheron's granulometry, which is however

[2] Sphericity is defined here in the sense given in the imageJ 3D Suite plugin documentation: it is the cubic root of the compactness C, which is computed from the volume V and the surface area S of an object, weighted so that it is 1 for a sphere ($C = 36\pi V^2/S^3$).

now based on inserted spheres and non longer disks. In this study, the samples are reduced to cubes of volume $V = 650\text{x}650\text{x}650\ \mu m^3$ for practical reasons: simpler boundary conditions, reduction of computational time and memory requirements. Note also that the porous networks studied here using XRCT images are not skeletonised, mainly because it is not an easy task to perform in 3D. However, it turns out that the length of the intercepts and the radius of the Matheron spheres are hardly affected by skeletonisation, since they aim at characterizing inter-pore spaces that are very wide compared to the thickness of the inter-granules pores.

The length of the intercepts is inherently a 1D data. Measuring this parameter in a 3D image therefore simply means measuring it along all possible directions, and in practice along the three axes of the images. Concerning Matheron's granulometry, the insertion of maximal spheres in the interpore spaces requires the full 3D distribution of pores. Since the investigated XRCT volumes are relatively small, edge effects are expected and need to be quantified. By studying the evolution of the measurement of the intercepts while progressively increasing the size of the observation window, we could show, by assuming periodicity and by attributing the size of the window to intercepts too large to be contained in the image, that the distribution functions obtained on reduced volumes remain consistent with those obtained on larger volumes, up to the size of the reduced volume. On the other hand, the calculation of the radius of Matheron spheres was only weakly dependent on window size, probably because the inserted spheres are strongly constrained by the presence of pores, and remain small with respect to window size for the tested range.

Figure 6 shows the cumulative distribution functions H_{Inter} and H_{Mat} measured on the XRCT images and on the tuned virtual microstructures (depicted in the top line of figure 5). The presence of vertical asymptotes in H_{Inter} measured from the XRCT images results from the above described treatment of intercepts larger than the size of the study window. Up to this limit, the cumulative distribution functions associated with the length of the intercepts measured on the real and virtual microstructures are in very good agreement for the C_1 and C_3 ceramics but, againg, not for C_2. This confirms the results obtained in the previous section when comparing the branch and primary branch lengths measured in 2D on OM and XRCT images (figure 3) and might be explained by long range fluctuations in the C_2 ceramic. Regarding the distribution of the radius of the Matheron spheres, the discrepancy which was already observed in 2D (section 3), is even more pronounced in 3D: virtual microstructures exhibit a too narrow distribution of Matheron spheres, with especially an underrepresentation of large spheres. This observation holds for all three ceramics and echoes the discussion in section 3 about the limitations of the simple geometric model used to generate the virtual microstructures, in particular the IGB model, and the conclusions drawn from it, conclusions that are all the more valid in 3D.

Virtual microstructures are fitted on data obtained from large 2D fields of observations of the ceramics under study. They therefore incorporate some large scale variations in the descriptor parameters: in particular the distribution of the lengths of the intercepts is well fitted by the virtual microstructures up to 2500 μm for ceramic C_1 and almost 2000 μm for C_2 and C_3 (see figure 2). In order to put into perspective the characterization carried out by XRCT on relatively small volumes, we measured

the length of the intercepts and the radius of Matheron's spheres in sub-volumes of size 650x650x650 µm^3, randomly extracted from the full volumes used for the optimisation process of size 3113x3113x3113 µm^3, and quantified the statistical fluctuations of their distribution functions, represented as uncertainty bars on the plots in figure 7). As expected, when the length of the intercepts reaches the size of the sub-volumes, the vertical asymptotes are observed as for the XRCT images. Before this limit, the values obtained for the reduced volumes and the full volumes are consistent. This consistency is also found for the radius of the Matheron spheres, now over the whole range of values. The distributions obtained over reduced volumes are therefore in very good agreement with those measured over full volumes, up to the limit imposed by their size. Statistical fluctuations observed between the different small sub-volumes of the virtual microstructures remain small, for both H_{Inter} and H_{Mat}. In particular, for the ceramic C_2, these variations are not large enough to contain the cumulative distribution function associated with the length of the intercepts measured on the XRCT image.

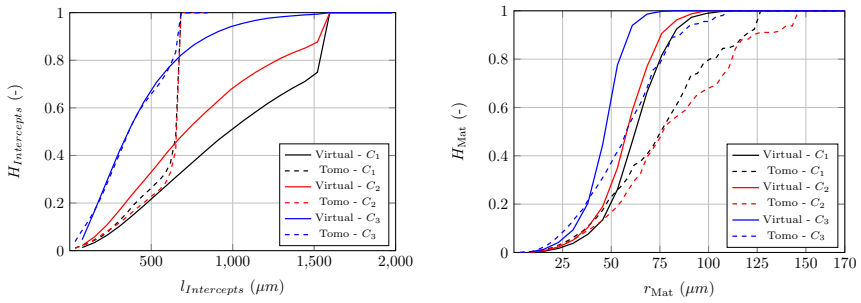

Fig. 6 Cumulative distribution functions H_{Inter} and H_{Mat} calculated on the XRCT images of the ceramics C_1, C_2 and C_3 as well as on the virtual microstructures associated with these ceramics, optimized on 2D data and simulated over 1556x1556x1556 µm^3 windows.

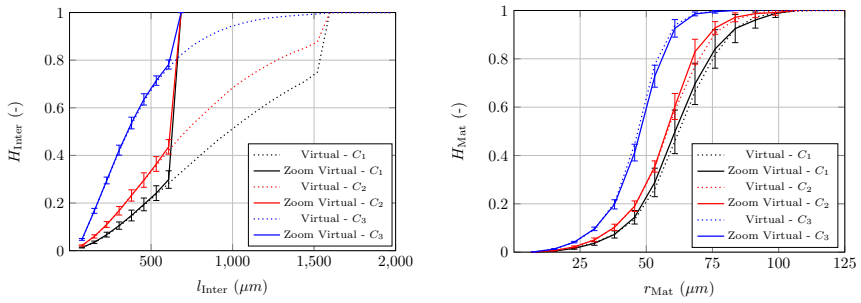

Fig. 7 Cumulative distribution functions H_{Inter} and H_{Mat} calculated on randomly chosen sub-volumes (650x650x650 µm^3) and on large volumes (1556x1556x1556 µm^3) of the optimized virtual microstructures associated with the ceramics of interest. Error bars quantify the fluctuations.

5 Conclusions

Using the optimisation process developed in [2], based on the method for generating virtual microstructures with inter-granules pores introduced in [1], 3D morphological models representative of the microstructures of UO_2 ceramics have been obtained. These models rely on a 2D characterisation of the ceramics based on OM images. In order to confirm their relevance, a validation based on XRCT images, providing 3D informations on the microstructures, has been proposed here. This 3D characterisation validates a posteriori the 2D characterisation carried out to date, as well as the proposed 3D morphological model, at least for some of the selected morphological parameters and for the smaller scales. Larger scales are not accessible with XRCT images, because of the limited size of the samples that can be imaged.

Acknowledgements This study was funded by the CEA and École des ponts (Grant 5765). The microstructures and the FFT computations were produced with version 1.0 of the MEROPE software and version 1.8 of the TMFFT software (components of the PLEIADES platform), respectively. The XRCT investigations were run in April 2022 at Synchrotron Soleil in the context of proposal 20211112. The authors are grateful to M. Soulon from CEA, who prepared the core samples as well as to V. Bouineau from CEA and P. Aimedieu, J. Archez, C. Doré-Ossipyan and N. Du from Laboratoire Navier for their contributions to the X-ray tomography campaign.

References

1. Meynard J, Ibrahim M, Monnier A, Bornert M, Castelier E et al (2022) Effective properties of an isotropic solid weakened by micro-cracks located at inter-granular boundaries. Journal of the Mechanics and Physics of Solids doi: 10.1016/j.jmps.2021.104647
2. Moutin L, Meynard J, Josien M, Bornert M et al (2023) Realistic morphological models of weakly to strongly branched pore networks for the computation of effective properties. International Journal of Solids and Structures doi: 10.1016/j.ijsolstr.2023.112249
3. Bargmann S, Klusemann B, Markmann J, Schnabel JE, Schneider K, Soyarslan C, Wilmers J (2018) Generation of 3D representative volume elements for heterogeneous materials: A review. Progress in Materials Science, 96:322–384
4. D. Jeulin (2000) Random texture models for material structures. Statistics and Computing doi: 10.1023/A:1008942325749
5. Bilger N, Auslender F, Bornert M, Michel J-C, Moulinec H, Suquet P and Zaoui A (2005) Effect of a nonuniform distribution of voids on the plastic response of voided materials: a computational and statistical analysis. International Journal of Solids and Structures 42(2):517–538.
6. Gasnier J B, Willot F, Trumel H, Jeulin D and Besson J (2018) Thermoelastic properties of microcracked polycrystals. Part I: Adequacy of Fourier-based methods for cracked elastic bodies. International Journal of Solids and Structures 155:248–256.
7. Bortolussi V, Figliuzzi B, Willot F, Faessel M and Jeandin M (2018) Morphological modeling of cold spray coatings. Image Analysis and Stereology 37(2):145–158.
8. Abrams H (1971) Grain size measurement by the intercept method. Metallography doi: 10.1016/0026-0800(71)90005-X
9. Matheron G. (1967) Éléments pour une théorie des milieux poreux. Masson, Paris
10. Sanchez S, Fernandez V, Pierce S and Tafforeau P (2013) Homogenization of sample absorption for the imaging of large and dense fossils with synchrotron microtomography. Nature Protocols doi: 10.1038/nprot.2013.098